Inorg. Chem. **2004**, *43*, 6195–6202

Design and Study of Bi[1,8]naphthyridine Ligands as Potential Photooxidation Mediators in Ru(II) Polypyridyl Aquo Complexes

Ruifa Zong,[†] Frederic Naud,[‡] Carrie Segal,[‡] John Burke,[‡] Feiyue Wu,[†] and Randolph Thummel*[,†]

Department of Chemistry, 136 Fleming Building, University of Houston, Houston, Texas 77204-5003, and Department of Chemistry, Trinity University, San Antonio, Texas 78212-7200

Received April 5, 2004

A series of 3,3′-polymethylene-bridged bi[1,8]naphthyridine (binap) ligands, **3a**–**c**, are complexed with Ru(II) to afford [Ru(tpy)(**3a**–**c**)(H_2O)]$^{2+}$ where an uncomplexed nitrogen on **3a**–**c** is situated so it can form a H-bond with the coordinated water. An additional complex involving [Ru(4′-NMe_2tpy)(**3b**)(H_2O)]$^{2+}$ is also prepared. X-ray analyses of the [Ru(tpy)(**3a**,**c**)(H_2O)]$^{2+}$ complexes indicate well-organized H-bonds even when the binap is nonplanar. In an attempt to realize photooxidation, the effects of light, varying potential, and pH were examined. A Pourbaix diagram indicated that the oxidation potential decreased by ∼0.5 V in the pH range of 1.9–11.6. The lowest-energy electronic absorption for the binap complexes involves the metal-to-ligand charge transfer to the binap ligand and is sensitive to ligand planarity. The absorbance shifted to a lower energy as the auxiliary ligand became a better donor (4′-NMe_2tpy) or as the water was deprotonated. Acetonitrile was found to displace water most easily for the complex of **3c**, where the ligand is the least planar. Despite promising features, photooxidation of the bound water was not observed.

Introduction

Considerable recent attention has been directed toward the use of hydrogen as a fuel.[1] The energy content of hydrogen is high, and the combustion product, water, is benign. No noxious byproducts are expected from this process. In fact, the use of hydrogen-powered fuel cells for automobiles is under discussion, and relatively short-term production goals are being considered.[2] What is conspicuously lacking is an economical, large-scale means of producing hydrogen.

An abundant potential source of hydrogen is water, and the most obvious economical means of decomposing water into its elements is through the utilization of solar radiation.[3] From the earliest times, nature has recognized this unavoidable mandate, and thus, photosynthesis is the principle source of biochemical energy. The challenge for modern science is to find practical methods for using solar energy in large-scale useful chemistry in vitro. For water decomposition, what is needed is a photocatalyst whose excited state can efficiently promote the bond-breaking and bond-making steps required for the production of hydrogen and oxygen.[4] Although hydrogen is the desired product, oxygen production is also required in order for the process to be truly catalytic.[5]

Numerous efforts at water decomposition have centered around the use of $[Ru(bpy)_3]^{2+}$ (bpy = 2,2′-bipyridine) as the photocatalyst.[6] However, the required redox chemistry must take place outside of the coordination sphere of the metal, and the mechanistic demands for this to occur

* Author to whom correspondence should be addressed. E-mail: Thummel@UH.edu.
[†] University of Houston.
[‡] Trinity University.

(1) (a) Jacoby, M. *Chem. Eng. News* **2003**, *81*, 35−36. (b) Veziroglu, T. N. *J. Adv. Sci.* **2001**, *13*, 101−116. (c) Veziroglu, T. N.; Barbir, F. *Int. J. Hydrogen Energy* **1992**, *17*, 391−404. (d) Momirlan, M.; Veziroglu, T. N. *Renewable Sustainable Energy Rev.* **2002**, *6*, 141−179. (e) *Advances in Hydrogen Energy*; Grégoire Padró, C. E., Lau, F., Eds.; Kluwer: New York, 2000.
(2) Schneider, P. B. G. *The Washington Post*, Jan 30, 2003, p A9.
(3) (a) Grätzel, M. *Acc. Chem. Res.* **1981**, *14*, 376−384. (b) Borgarello, E.; Kiwi, J.; Pelizzetti, E.; Visca, M.; Grätzel, M. *J. Am. Chem. Soc.* **1981**, *103*, 6324−6329. (c) Domen, K.; Kondo, J. N.; Hara, M.; Takata, T. *Bull. Chem. Soc. Jpn.* **2000**, *73*, 1307−1331.
(4) (a) Morris, N. D.; Mallouk, T. E. *J. Am. Chem. Soc.* **2002**, *124*, 11114−11121. (b) Chronister, C. W.; Binstead, R. A.; Ni, J.; Meyer, T. J. *Inorg. Chem.* **1997**, *36*, 3814−3815. (c) Binstead, R. A.; Chronister, C. W.; Ni, J.; Hartshorn, C. M.; Meyer, T. J. *J. Am. Chem. Soc.* **2000**, *122*, 8464−8473. (d) Lehn, J.-M.; Sauvage, J.-P.; Ziessel, R. *New J. Chem.* **1979**, *3*, 423−427.
(5) (a) Wada, T.; Tsuge, K.; Tanaka, K. *Angew. Chem., Int. Ed.* **2000**, *39*, 1479−1482. (b) Naruta, Y.; Sasayama, M.-A.; Sasaki, T. *Angew. Chem., Int. Ed. Engl.* **1994**, *33*, 1839−1840. (c) Yagi, M.; Wolf, K. V.; Baesjou, P. J.; Bernasek, S. L.; Dismukes, G. C. *Angew. Chem., Int. Ed.* **2001**, *40*, 5925−5928.

10.1021/ic040051n CCC: $27.50
Published on Web 09/03/2004

effectively for the simple parent system are severe. Alternatively, one might coordinate a water molecule directly to the metal center. Oxidation would then lead to a metal−oxo species, with the concurrent evolution of hydrogen. This process would be followed by O−O bond-forming steps, which could occur either by hydration or by dimerization of the metal−oxo moiety.

Initially, we propose to stay close to the $[Ru(bpy)_3]^{2+}$ prototype by merely replacing a pyridine ligand with water. The $[Ru(bpy)(tpy)(H_2O)]^{2+}$ complex (tpy = 2,2′;6′,2″-terpyridine) has been extensively studied by Meyer and others,[7] and at a pH of 7, a potential of 0.49 V will oxidize the system to the Ru(III)−OH species and 0.62 V will produce Ru(IV)═O. The challenge is to accomplish these same steps by using the photochemical energy that is available through the excited state of the complex.

The lowest-energy excited state for Ru(II) polypyridyl complexes is a metal-to-ligand charge-transfer (MLCT) state where photoexcitation promotes an electron from a metal d orbital to a π^* orbital on the most electronegative ligand.[8] In the excited state, this ligand is effectively reduced and, therefore, its proton affinity should be enhanced.[9] We would like to use this more basic, photoreduced ligand to assist with the deprotonation of a metal-bound water molecule[10] and, thus, promote effective photooxidation of the system.

This objective requires that either the bpy or the tpy ligand be redesigned to make it more electronegative and, thus, a good charge acceptor in the excited state. Furthermore, the same ligand must possess an available basic site proximal to the bound water. In this paper, we describe the use of a series of 3,3′-polymethylene-bridged derivatives of 2,2′-bi-[1,8]naphthyridine (**3a**−**c**) for this purpose.[11]

Experimental Section

^{1}H NMR spectra were measured at 300 MHz on a General Electric QE-300 spectrometer. Chemical shifts are reported in parts per million relative to TMS. UV−vis spectra were recorded on a Perkin-Elmer Lambda-3B spectrometer. Emission spectra were obtained on a Perkin-Elmer LS-50B luminescence spectrometer equipped with a Hamamatsu R928HA photomultiplier tube. Cyclic voltammetric measurements were carried out by using a BAS Epsilon electroanalytical system. The CV experiments were performed in a one-compartment cell equipped with a glassy carbon working electrode, a saturated calomel reference electrode (SCE), and a Pt wire as the auxiliary electrode. UV−vis spectroelectrochemical experiments were performed in dichloromethane containing 0.2 M tetrabutylammonium hexafluorophosphate using an optically transparent platinum thin-layer electrode.[12] Potentials were applied with an EG&G model 173 potentiostat. Time-resolved UV−vis spectra were recorded with a Hewlett-Packard model 8453 diode array rapid-scanning spectrophotometer. Mass spectra were recorded on a Finnigan MAT model SSQ 700 quadrupole mass spectrometer fitted with an electrospray ionization source. The electrospray voltage was −3.5 kV. Samples were introduced by the direct infusion of a solution at a concentration of $\sim 5 \times 10^{-11}$ mol/L at a flow rate of 1 μL/min. Spectra were acquired after signal averaging for several minutes. Infrared spectra were recorded on a Thermo Nicolet AVATAR 370 FT-IR spectrometer. Elemental analyses were performed by QTI. The 3,3′-dimethylene-2,2′-binaphthyridine (**3a**),[11] 3,3′-trimethylene-2,2′-binaphthyridine (**3b**),[11] 3,3′-tetramethylene-2,2′-binaphthyridine (**3c**),[11] $[Ru(tpy)Cl_3]$,[13] and $[Ru(4'\text{-}NMe_2tpy)Cl_3]$[14] were prepared by following the literature methods.

[Ru(tpy)(3a)(H$_2$O)](PF$_6$)$_2$. A mixture of $Ru(tpy)Cl_3$ (263 mg, 0.6 mmol) and 3,3′-dimethylene-2,2′-binaphthyridine (166 mg, 0.58 mmol) in ethanol/water (30:10 mL) and triethylamine (0.3 mL) was refluxed for 4 h. The solution was concentrated to about 5 mL, and then, NH_4PF_6 (280 mg, 1.57 mmol) in water (3 mL) was added. The solution was stirred for 30 min, and the solvent evaporated. The crude product, dissolved in a minimum amount of acetone, was purified by column chromatography (alumina, eluting with acetone/hexanes). Impurities as pink, blue, and orange fractions were eluted first with a 1:1 ratio of acetone/hexanes. A green fraction was recovered with acetone, and the crude product was recrystallized from acetone/water to give fine green crystals, which were dried in vacuo overnight (338 mg, 61%). ^{1}H NMR (acetone-d_6): δ 9.28 (dd, J = 4.5, 1.8 Hz, 1H), 9.10 (dd, J = 8.4, 1.8 Hz, 1H), 8.96 (s, 1H), 8.84 (d, J = 7.8 Hz, 2H), 8.62 (dd, J = 7.8, 1.2 Hz, 2H), 8.48 (t, J = 7.8 Hz, 1H), 8.33 (dd, J = 6.6, 1.5 Hz, 1H), 8.32 (s, 1H), 8.28 (s, 1H), 8.16 (dd, J = 7.8, 4.5 Hz, 1H), 7.98 (td, J = 8.1, 1.5 Hz, 2H), 7.95 (s, 1H), 7.90 (d, J = 5.4 Hz, 2H), 7.55 (dd, J = 7.8, 4.2 Hz, 1H), 7.23 (m, 2H), 3.75 (q, 2H), 3.57 (q, 2H). MS (ESI): m/z 782 ($[M - PF_6]^+$), 638 ($[M - 2PF_6]^+$). IR (ATR, cm^{-1}): ν 1606 (vw), 1450 (vw), 837 (vs), 769 (m). Anal. Calcd for $C_{33}H_{25}F_{12}N_7OP_2Ru\cdot H_2O$: C, 41.96; H, 2.67; N, 10.38. Found: C, 42.03; H, 2.32; N, 10.15.

[Ru(tpy)(3b)(H$_2$O)](PF$_6$)$_2$. The same procedure was followed as described for $[Ru(tpy)(\mathbf{3a})(H_2O)](PF_6)_2$, using $Ru(tpy)Cl_3$ (220 mg, 0.5 mmol), 3,3′-trimethylene-2,2′-binaphthyridine (150.0 mg, 0.5 mmol), and NH_4PF_6 (256 mg, 1.57 mmol) to afford dark-green crystals (329 mg, 70%). ^{1}H NMR (acetone-d_6): δ 9.32 (dd, J = 4.5, 1.8 Hz, 1H), 9.14 (dd, J = 7.8, 1.8 Hz, 1H), 9.03 (s, 1H), 8.79 (d, J = 8.1 Hz, 2H), 8.58 (d, J = 8.1 Hz, 2H), 8.43 (t, J = 8.1 Hz, 1H), 8.35 (m, 2H), 8.33 (s, 1H), 8.20 (dd, J = 8.4, 4.5 Hz, 1H), 7.98 (dt, J = 7.8, 1.8 Hz, 2H), 7.91 (d, J = 4.8 Hz, 2H), 7.78 (s, 1H), 7.55 (dd, J = 8.1, 4.2 Hz, 1H), 7.24 (m, 2H), 3.19 (m, 4H), 2.68 (m, J = 7.2 Hz, 2H). IR (ATR, cm^{-1}): ν 1698 (w), 1606 (vw), 1450 (w), 836 (vs), 770 (m). Anal. Calcd for $C_{34}H_{27}F_{12}N_7OP_2Ru\cdot 0.5C_3H_6O\cdot H_2O$: C, 43.17; H, 3.26; N, 9.93. Found: C, 42.77; H, 3.05; N, 9.59.

[Ru(tpy)(3c)(H$_2$O)](PF$_6$)$_2$. The same procedure as described for $[Ru(tpy)(\mathbf{3a})(H_2O)](PF_6)_2$ was followed, using $Ru(tpy)Cl_3$ (236 mg,

(6) (a) Abruna, H. D.; Teng, A. Y.; Samuels, G. J.; Meyer, T. J. *J. Am. Chem. Soc.* **1979**, *101*, 6745−6746. (b) Meyer, T. J. *Acc. Chem. Res.* **1989**, *22*, 163−170. (c) Sprintschnik, G.; Sprintschnik, H. W.; Kirsch, P. P.; Whitten, D. G. *J. Am. Chem. Soc.* **1976**, *98*, 2337−2338. (d) Krishnan, C. V.; Brunschwig, B. S.; Creutz, C.; Sutin, N. *J. Am. Chem. Soc.* **1985**, *107*, 2005−2015. (e) Sun, L.; Hammerström, L.; Åkermark, B.; Styring, S. *Chem. Soc. Rev.* **2001**, *30*, 36−49.

(7) (a) Takeuchi, K. J.; Thompson, M. S.; Pipes, D. W.; Meyer, T. J. *Inorg. Chem.* **1984**, *23*, 1845−1851. (b) Trammell, S. A.; Wimbish, J. C.; Odobel, F.; Gallagher, L. A.; Narula, P. M.; Meyer, T. J. *J. Am. Chem. Soc.* **1998**, *120*, 13248−13249.

(8) (a) Kalyanasundaram, K. *Photochemistry of Polypyridine and Porphyrin Complexes*; Academic Press: San Diego, CA, 1992. (b) Juris, A.; Balzani, V.; Barigelletti, F.; Campagna, S.; Belser, P.; von Zelewsky, A. *Coord. Chem. Rev.* **1988**, *84*, 85−277.

(9) Dougherty, T.; Hicks, C.; Maletta, A.; Fan, J.; Rutenberg, I.; Gafney, H. D. *J. Am. Chem. Soc.* **1998**, *120*, 4226−4227.

(10) Watts, R. J.; Bergeron, S. F. *J. Phys. Chem.* **1979**, *83*, 424−425.

(11) Thummel, R. P.; Lefoulon, F.; Cantu, D.; Mahadevan, R. *J. Org. Chem.* **1984**, *49*, 2208−2212.

(12) Lin, X. Q.; Kadish, K. M. *Anal. Chem.* **1985**, *57*, 1498−1501.

(13) Sullivan, B. P.; Calvert, J. M.; Meyer, T. J. *Inorg. Chem.* **1980**, *19*, 1404−1407.

(14) Constable, E. C.; Cargill Thompson, A. M. W.; Tocher, D. A.; Daniels, M. A. M. *New J. Chem.* **1992**, *16*, 855−867.

Table 1. Data Collection and Processing Parameters for [Ru(tpy)(**3a**)(H_2O)](PF_6)$_2$·(C_3H_6O) and [Ru(tpy)(**3c**)(H_2O)](ClO_4)$_2$·H_2O

	[Ru(tpy)(**3a**)(H_2O)](PF_6)$_2$·(C_3H_6O)	[Ru(tpy)(**3c**)(H_2O)](ClO_4)$_2$·H_2O
molecular formula	$C_{36}H_{31}F_{12}N_7O_2P_2Ru$	$C_{35}H_{31}Cl_2N_7O_{10}Ru$
formula weight	984.75	881.64
space group	$P\bar{1}$ (triclinic)	$P2_1/c$ (monoclinic)
cell constants	a = 8.664(1) Å	8.6587(4) Å
	b = 10.613(1) Å	25.6328(11) Å
	c = 21.264(3) Å	16.3548(7) Å
	α = 100.28°	90.00°
	β = 93.86°	103.281(1)°
	γ = 95.99°	90.00°
formula units per cell, Z	2	4
volume (Å^3)	1906	3532.8(3)
density, ρ (g/cm^3)	1.72	1.658
absorption coefficient, μ (cm^{-1})	5.86	0.666
temperature, T (K)	223(2)	223(2)
radiation, λ (Mo Kα, Å)	0.71073	0.71073
collection range	4° ≤ 2θ ≤ 50°	3° ≤ 2θ ≤ 47°
scan width	$\Delta\theta = 1.25 + (K\alpha_2 - K\alpha_1)$°	
scan speed range (deg min^{-1})	1.5−15.0	
total data collected	6723	16358
independent data	5699	5373
total variables	561	479
R1	0.028 with $I > 3\sigma(I)$	0.039 with $I > 4\sigma(I)$
wR	0.028	
wR2		0.095

0.53 mmol), 3,3′-tetramethylene-2,2′-binaphthyridine (156 mg, 0.5 mmol), and NH_4PF_6 (256 mg, 1.57 mmol) to provide 359 mg (75%) of the complex. ^{1}H NMR (acetone-d_6, −50 °C): δ 9.34 (d, J = 3.0 Hz, 1H), 9.14 (d, J = 9.0 Hz, 1H), 9.13 (s, 1H), 8.92 (d, J = 7.8 Hz, 1H), 8.76 (d, J = 7.8 Hz, 1H), 8.70 (d, J = 7.8 Hz, 1H), 8.44 (m, 2H), 8.42 (m, 1H), 8.35 (s, 1H), 8.34 (s, 1H), 8.20 (dd, J = 4.2, 8.1 Hz, 1H), 8.05 (t, J = 7.8 Hz, 1H), 7.94 (d, J = 8.1 Hz, 2H), 7.61 (d, J = 5.1 Hz, 1H), 7.54 (dd, J = 4.5, 7.5 Hz, 1H), 7.27 (m, 2H), 3.11 (m, 2H), 3.01 (m, 2H), 2.73 (m, 2H), 2.35 (m, 2H). IR (ATR, cm^{-1}): ν 1698 (vw), 1599 (vvw), 1449 (vw), 838 (vs), 771 (m). Anal. Calcd for $C_{35}H_{29}F_{12}N_7OP_2Ru$: C, 44.03; H, 3.06; N, 10.27. Found: C, 44.24; H, 3.23; N, 10.03.

[Ru(4′-NMe_2tpy)(3b)(H_2O)](PF_6)$_2$. The same procedure was followed as described for [Ru(tpy)(**3a**)(H_2O)](PF_6)$_2$, using [Ru(4′-NMe_2tpy)Cl_3] (113 mg, 0.23 mmol), 3,3′-trimethylene-2,2′-binaphthyridine (69 mg, 0.23 mmol), and NH_4PF_6 (109 mg, 0.6 mmol) to yield 117 mg (52%) of the product. ^{1}H NMR (acetone-d_6): δ 9.30 (dd, J = 4.5, 2.1 Hz, 1H), 9.08 (dd, J = 8.1, 1.8 Hz, 1H), 8.91 (s, 1H), 8.52 (d, J = 7.8 Hz, 2H), 8.47 (dd, J = 4.5, 2.1 Hz, 1H), 8.32 (dd, J = 8.2, 1.8 Hz, 1H), 8.18 (s, 1H), 8.15 (dd, J = 8.1, 4.5 Hz, 1H), 8.04 (s, 2H), 7.88 (dt, J = 7.8, 1.5 Hz, 2H), 7.81 (d, J = 4.8 Hz, 2H), 7.79 (s, 1H), 7.53 (dd, J = 8.2, 4.5 Hz, 1H), 7.13 (m, 2H), 3.52 (s, 6H), 3.17 (m, 4H), 2.68 (t, J = 7.2 Hz, 2H). IR (ATR, cm^{-1}): ν 1622 (vw), 1526 (vw), 1450 (vw), 1432 (vvw), 837 (vs), 779 (w). Anal. Calcd for $C_{36}H_{32}F_{12}N_8OP_2Ru$·$C_3H_6O$·$H_2O$: C, 44.20; H, 3.80; N, 10.57. Found: C, 43.90; H, 3.39; N, 10.33.

X-ray Analyses. A dark-red needle of [Ru(tpy)(**3a**)(H_2O)](PF_6)$_2$·(C_3H_6O), having the approximate dimensions of 0.10 × 0.20 × 0.80 mm^3, was mounted in a random orientation on a Nicolet R3m/V automatic diffractometer. The crystal was placed in a stream of dry nitrogen gas at −50 °C, and the radiation used was Mo Kα monochromatized by a highly ordered graphite crystal. Final cell constants and other information pertinent to the data collection and refinement are listed in Table 1. The Laue symmetry was determined to be $\bar{1}$, and the space group was shown to be either $P1$ or $P\bar{1}$. Intensities were measured using the omega-scan technique, with the scan rate depending on the count obtained in the rapid prescans of each reflection. Two standard reflections were monitored after every 2 h or every 100 data collected, and these showed no significant change. During data reduction, Lorentz and polarization corrections were applied; however, no correction for absorption was made due to the small absorption coefficient. Since the unitary structure factors displayed centric statistics, space group $P\bar{1}$ was assumed from the outset. The structure was solved by the interpretation of the Patterson map, which revealed the position of the Ru atom. Remaining non-hydrogen atoms were located in subsequent difference Fourier syntheses. The usual sequence of isotropic and anisotropic refinement was followed, after which all non-water hydrogens were entered in ideal calculated positions and constrained to riding motion, with a single variable isotropic temperature factor for all of them. The hydrogens on water were located in a difference map and refined independently with fixed isotropic temperature factors. One of the two independent anions was found to be disordered, having a major orientation (75% occupancy) and a minor orientation (25% occupancy). This was treated by introducing a rigid-body model having isotropic thermal parameters in the minor orientation. After all shift/esd ratios were <0.1, convergence was reached at the agreement factors listed in Table 5. No unusually high correlations were noted between any of the variables in the last cycle of the full-matrix least-squares refinement, and the final difference density map showed a maximum peak of ∼0.5 e/Å^3. All calculations were made using Nicolet's SHELXTL PLUS (1987) series of crystallographic programs.[15]

A dark-purple crystal of [Ru(tpy)(**3c**)(H_2O)](ClO_4)$_2$·H_2O, with the dimensions of 0.20 × 0.15 × 0.15 mm^3, was measured with a Siemens SMART platform diffractometer equipped with a 1K CCD area detector. A hemisphere of data (1271 frames at a 5 cm detector distance) was collected using a narrow-frame method with scan widths of 0.30° in omega and an exposure time of 30 s/frame. The first 50 frames were remeasured at the end of data collection to monitor the instrument and crystal stability, and the maximum correction on I was <1%. The data were integrated using the Siemens SAINT program, with the intensities corrected for Lorentz factor, polarization, air absorption, and absorption due to variation in the path length through the detector faceplate. A psi-scan absorption correction was applied based on the entire data set. Redundant reflections were averaged. Final cell constants were

(15) Sheldrick, G. M. In *Crystallographic Computing 3*; Sheldrick, G. M., Kruger, C., Goddard, R., Eds.; Oxford University Press: Oxford, U.K., 1985; pp 175−189.

Scheme 1

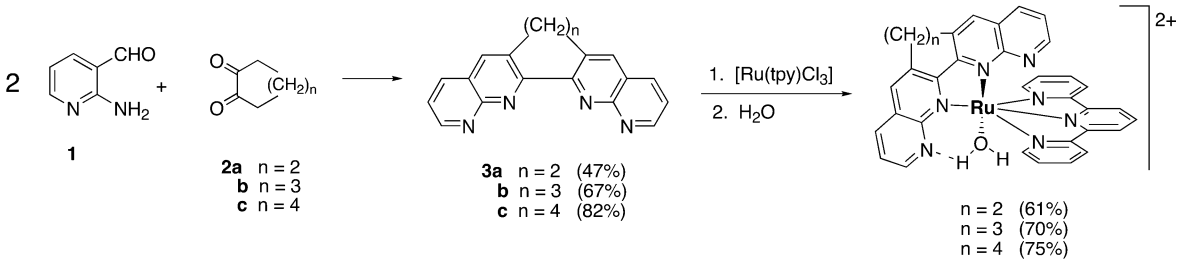

Scheme 2

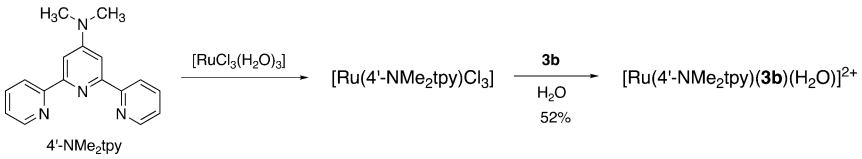

refined using 7076 reflections having $I > 10\sigma(I)$, and these, along with other information pertinent to data collection and refinement, are listed in Table 1. The Laue symmetry was determined to be 2/*m*, and from the systematic absences noted, the space group was shown unambiguously to be $P2_1/c$. One of the two perchlorate anions is disordered over two slightly different positions, and this was treated using ideal rigid-body models. Both water molecules were also treated as ideal rigid bodies and were allowed to refine independently. The structure was refined by SHELXL-97,[16] and the final difference density map showed a maximum peak of 0.773 e/Å^3.

Results and Discussion

The bridged binaphthyridine (binap) ligands **3a**−**c** were synthesized in good yields by the Friedländer condensation of 2-aminonicotinaldehyde (**1**) with a series of 1,2-cycloalkanediones (**2a**−**c**) according to a procedure which has been reported earlier.[11] The complexes were prepared by treating the ligands with [Ru(tpy)Cl_3] in aqueous ethanol in the presence of triethylamine and precipitated as their hexafluorophosphate salts (Scheme 1). Purification was effected by the chromatography on alumina and recrystallization. To help evaluate the influence of the tpy ligand we also prepared 4′-dimethylamino-tpy according to a literature procedure.[14] This ligand was then used to prepare the [Ru(4′-NMe_2tpy)-Cl_3] reagent by reacting it with [$RuCl_3(H_2O)_3$] in the customary fashion (Scheme 2). Subsequent reaction with **3b** in aqueous ethanol led to the corresponding binap complex in 52% yield. It is interesting that the binaps only show products resulting from complexation of the interior nitrogens (N1, N1′), although one might expect the exterior nitrogens (N8, N8′) to be more accessible. The stability provided by a five-membered chelate ring formation is the dominant effect. The formation of a four-membered chelate involving N1 and N8 is much less likely.[17] Since the binap ligands exhibit C_2 symmetry, a single isomer of the product results.

For the parent system, [Ru(tpy)(bpy)$(H_2O)]^{2+}$, the initially formed species is the chloro complex, which can only be hydrated with the assistance of silver to ionize the Ru−Cl bond.[7a] The binap systems, however, hydrate spontaneously under the reaction conditions, promoted by anchimeric assistance from the uncomplexed N3. This assistance is manifested both by electrostatic repulsion of the chloride leaving group and by stabilization of the incoming water through hydrogen bonding. Even in the presence of added LiCl, only the aquo complex was obtained.

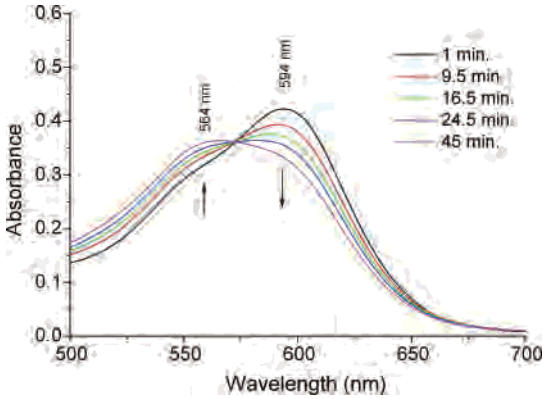

Figure 1. Electronic absorption spectrum of [Ru(tpy)(**3b**)$(H_2O)](PF_6)_2$ (7.5×10^{-5} M, 4 mL of acetone) with added acetonitrile (25 μL) recorded as a function of time.

Initial attempts to measure the NMR spectra of these complexes in CD_3CN showed that the spectra changed with time, indicating solvolysis of the bound water which was being replaced by acetonitrile. When an acetone solution of [Ru(tpy)(**3b**)$(H_2O)]^{2+}$ is exposed to added acetonitrile, the absorption spectrum changes with time. The peak at 594 nm disappears, and the peak at 564 nm increases in intensity (Figure 1).

The complexes are characterized by their ^{1}H NMR spectra in acetone-d_6, which show signals that are both well-resolved and dispersed for the complexes of **3a** (Figure 2) and **3b**. Due to the conformational mobility of ligand **3c**,[18] this complex only became well-resolved at −50 °C. The complexes exhibit symmetry with respect to the tpy ligand so that all of the tpy signals, except the central Ha, integrate for two protons. The binap ligand is unsymmetrically bound

(16) Sheldrick, G. M. *SHELX-97*; University of Göttingen: Göttingen, Germany, 1997.
(17) Staniewicz, R. J.; Hendricker, D. G. *J. Am. Chem. Soc.* **1977**, *99*, 6581−6588.
(18) Thummel, R. P.; Lefoulon, F. *Inorg. Chem.* **1987**, *26*, 675−680.

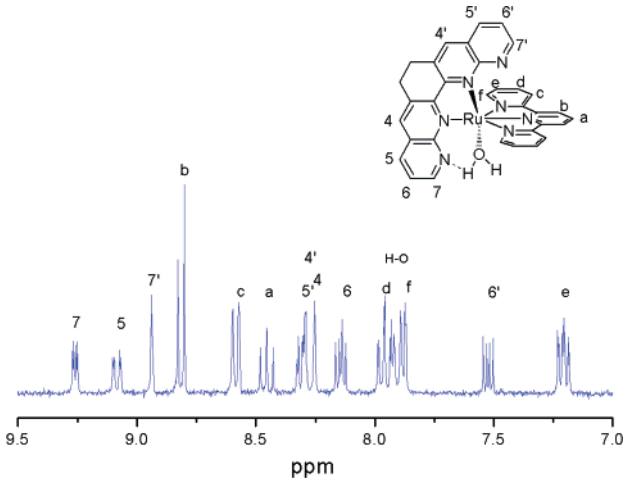

Figure 2. ^{1}H NMR spectrum of [Ru(tpy)(**3a**)(H_2O)](PF_6)$_2$ in acetone-d_6 at 298 K.

Table 2. ^{1}H NMR Data for Ligands **3a**−**c** and Their Ru(II) Complexes[a]

compound	H7	H6	H5	H4	H7′	H6′	H5′	H4′
3a	9.23	7.50	8.18	8.12				
3b	9.26	7.56	8.30	8.13				
3c	9.12	7.48	8.21	8.09				
[Ru(tpy)(**3a**)(H_2O)]$^{2+}$	9.28	8.16	9.10	8.32	8.96	7.54	8.33	8.28
[Ru(tpy)(**3b**)(H_2O)]$^{2+}$	9.32	8.20	9.14	8.35	9.03	7.55	8.35	8.33
[Ru(tpy)(**3c**)(H_2O)]$^{2+}$	9.34	8.20	9.14	8.35	9.13	7.54	8.34	8.34
[Ru(4′-NMe_2tpy)(**3b**)(H_2O)]$^{2+}$	9.30	8.15	9.08	8.16	8.91	7.53	8.32	8.47

[a] Recorded in $(CD_3)_2CO$ at 25 °C and reported in parts per million relative to TMS. Atom numbering scheme from Figure 2.

Table 3. Selected Structural Data for [Ru(tpy)(L)(H_2O)]$^{2+}$ (L = **3a** or **3c**)

[Ru(tpy)(**3a**)(H_2O)]$^{2+}$		[Ru(tpy)(**3c**)(H_2O)]$^{2+}$	
bond lengths (Å)			
Ru−N1	2.103(2)	Ru−N1	2.104(4)
Ru−N20	2.052(2)	Ru−N22	2.069(4)
Ru−N23	2.065(2)	Ru−N25	2.061(4)
Ru−N30	1.969(2)	Ru−N31	1.954(4)
Ru−N40	2.074(2)	Ru−N37	2.066(4)
Ru−O1	2.123(2)	Ru−O1	2.116(3)
N3−O1	2.657	N3−O1	2.644(5)
bond angles (deg)			
N1−Ru−O1	96.2(1)	N1−Ru−O1	96.67(13)
N1−Ru−N20	78.7(1)	N1−Ru−N22	78.26(14)
torsion angles (deg)			
N1−C22−C21−N20	8.7	N1−C24−C23−N22	29.3(5)
C9−C22−C21−C12	13.0	C9−C24−C23−C14	40.6(7)
O1−Ru−N1−C2	12.3	O1−Ru−N1−C2	10.8(4)

with one-half of the molecule being held closer to the orthogonal tpy ligand. The binap protons are assigned by a consideration of shielding effects and an analysis of their 2D-COSY spectra, and the data are summarized in Table 2. The H7′ proton points toward the face of the central pyridine ring of the orthogonal tpy ligand, causing it to be shielded and shifted upfield by 0.23−0.35 ppm. The effect is somewhat diminished for the more remote H6′. The remaining protons all experience downfield coordination-induced chemical shifts due to the electronic depletion resulting from complexation (H4 and H4′) and hydrogen bonding with the coordinated water (H5, H6, and H7). Singlets observed at 7.95, 7.78, and 7.79 for complexes [Ru(tpy)(**3a**,**b**)(H_2O)]$^{2+}$ and [Ru(4′-NMe_2tpy)(**3b**)(H_2O)]$^{2+}$ disappear upon the addition of D_2O, identifying them as belonging to the coordinated water.

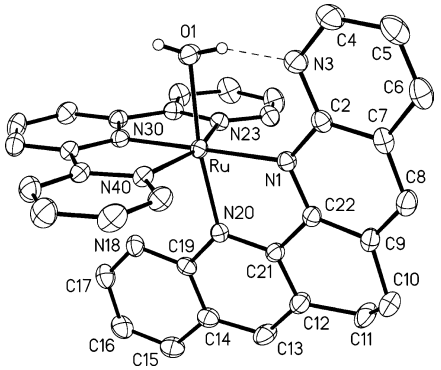

Figure 3. X-ray crystal structure of the cation of [Ru(tpy)(**3a**)(H_2O)](PF_6)$_2$·(C_3H_6O) with the atom numbering scheme.

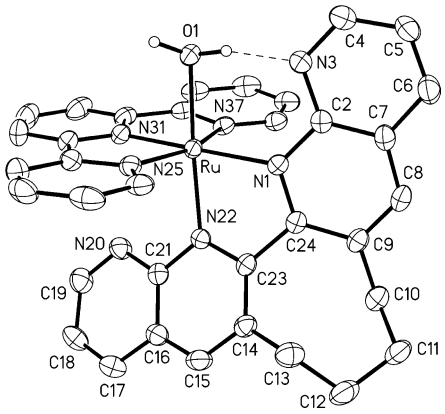

Figure 4. X-ray crystal structure of the cation of [Ru(tpy)(**3c**)(H_2O)]-(ClO_4)$_2$·H_2O with the atom numbering scheme.

To better understand the geometry of these complexes, especially with regard to the bound water molecule, we undertook single-crystal X-ray analyses of [Ru(tpy)(**3a**)-(H_2O)]$^{2+}$ and [Ru(tpy)(**3c**)(H_2O)]$^{2+}$. Some of the pertinent geometric data are summarized in Table 3, and the ORTEP plots for both cations are illustrated in Figures 3 and 4. The main difference between these two systems is the length of the polymethylene bridge connecting C3 and C3′ of the binap ligand. For the dimethylene-bridged free ligand **3a**, we have estimated a dihedral angle of about 18° between the two naphthyridine halves of the molecule.[19] This angle is flattened somewhat in the complex. Taking the average of the interior (N20, C21, C22, and N1) and exterior (C12, C21, C22, and C9) torsion angles, we find a dihedral angle of 11°. For the tetramethylene-bridged free ligand **3c**, we estimate a torsion angle of 58°[19] and thus would expect twisting of N3 away from the coordinated water, weakening this hydrogen bond. However, due to the constraints of the five-membered chelate ring, the ligand flattens considerably in the complex so that the average of the interior (N1, C24, C23, and N22) and exterior (C9, C24, C23, and C14) angles is 35°. The extent to which N3 might lie outside the plane containing O1, Ru, and N1 can be estimated from the torsion angle O1−Ru−N1−C2, which surprisingly is found to be 1.5° less than that for the dimethylene-bridged system. Apparently, there is

(19) Thummel, R. P. *Tetrahedron* **1991**, *47*, 6851−6886.

Table 4. Electronic Absorption and Emission Data for Binap-*n* and Their Ru(II) Complexes[a]

compound	λ_{max} (log ϵ)[b]		λ_{em}[c]
3a	362 (4.40)		
3b	325 (4.39)		
3c	321 (4.36)		
$[Ru(tpy)(\mathbf{3a})(H_2O)]^{2+}$	426 (3.75)	601 (4.03)	745
$[Ru(tpy)(\mathbf{3b})(H_2O)]^{2+}$	426 (3.91)	597 (3.98)	738
$[Ru(tpy)(\mathbf{3c})(H_2O)]^{2+}$	435 (3.98)	593 (3.93)	738
$[Ru(4'\text{-}NMe_2tpy)(\mathbf{3b})(H_2O)]^{2+}$	441 (4.07)	622 (4.00)	
$[Ru(tpy)(bpy)(H_2O)]^{2+}$	509 (4.05)		

[a] Wavelength reported in nanometers (nm). [b] At 5×10^{-5} M in CH_2Cl_2 at 298 K. [c] In 4:1 ethanol/methanol at 77 K.

a countering effect provided by an increased flexibility in this larger system. The H bond length can also be evaluated by considering the N3−O1 distance, which is nearly equal for both systems and leads to an estimate of ∼1.8 Å for the H bond. The coordinative bond lengths are comparable for the two complexes, with the central Ru−N bond of the tpy being the shortest, as expected.

Spec and co-workers have examined the structure of a similar $[Ru(tpy)(biq)Cl]^+$ system involving 2,2′-biquinoline (biq) in place of binap.[20] Using the same preparative procedure, they do not obtain the aquo complex, whereas for our systems, just the opposite is found. We get only the aquo complex and are unable to isolate the chloro system. The dihedral angle between the two quinoline rings, determined as an average of interior and exterior angles, is 10.6° and very similar to that of our dimethylene-bridged system. Spek shows that the C8−H bond on one quinoline is pointing toward the Cl atom with an H8−Cl distance of 2.5 Å, which is quite a bit longer than that of the H-bonded situation found in the binap systems. For the biq system, this congestion is suggested to reduce the reactivity of the chloride, while for naphthyridine, this reactivity is enhanced.

The absorption and emission spectral data for the 1,8-binaphthyridine ligands and their complexes are summarized in Table 4. For the complexes examined in this study, the bpy ligand of the parent $[Ru(tpy)(bpy)(H_2O)]^{2+}$ complex has been replaced by a bridged binap in an effort to direct MLCT primarily to this ligand. Binap may be considered as a dipyrido-fused analogue of bpy, which is both more delocalized and more electronegative, making it a much better charge acceptor.[21] This difference is evidenced by the absorption maxima of the free ligands, where the bpy long wavelength absorption is at 284 nm[22] and the binaps absorb at 321−362 nm. It is noteworthy that the more planar system, profiting from better delocalization, has the lowest-energy absorption.

The difference in the electronegativity of binap versus tpy becomes apparent when one examines the absorption spectra of the $[Ru(tpy)(\mathbf{3a-c})(H_2O)]^{2+}$ complexes, which show a long wavelength component at 593−601 nm for MLCT to the binap ligand and a shorter wavelength band at 426−435 nm for MLCT to the tpy ligand. This same trend has been observed earlier for MLCT in the mixed-ligand $[Ru(\mathbf{3a-c})(bpy)_2]^{2+}$ complexes.[18] Figure 5 illustrates the interplay between the two MLCT components of the absorption. The three homologous binap complexes show a steady decrease in the intensity of the long wavelength band as the 3,3′-bridge increases in length and the binap ligand becomes less planar. At the same time, the higher-energy tpy component steadily increases in intensity.[23] For the parent system, the bpy component dominates with a strong absorption band at 509 nm and only a very small shoulder for tpy at ∼450 nm. The $[Ru(4'\text{-}NMe_2tpy)(\mathbf{3b})(H_2O)]^{2+}$ complex shows somewhat unusual behavior. One would expect the electron-donating dimethylamino substituent to inhibit MLCT into the tpy ligand. However, the 4′-NMe_2tpy MLCT component is more intense than the components for any of the simple tpy complexes. In addition, the binap-3 component is shifted 25 nm to a lower energy. The bridged binap complexes were found to be nonemissive at room temperature and only weakly emissive at 77 K. As expected, the more planar complex of **3a** showed the lowest-energy emission.

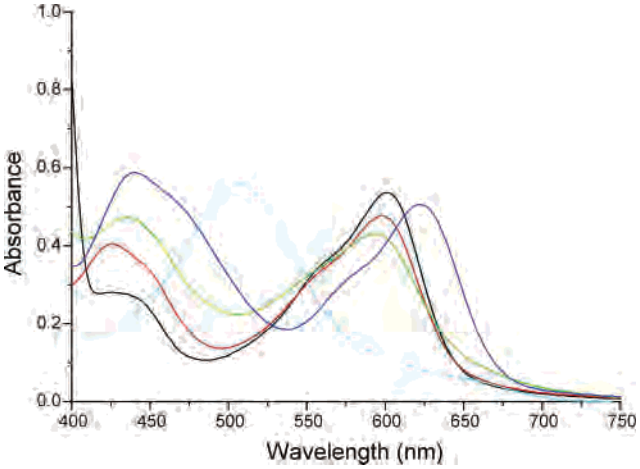

Figure 5. Visible absorption spectra of $[Ru(tpy)(L)(H_2O)]^{2+}$, L = **3a** (black), **3b** (red), and **3c** (green); $[Ru(4'\text{-}NMe_2tpy)(\mathbf{3b})(H_2O)]^{2+}$ (blue); and $[Ru(tpy)(bpy)(H_2O)]^{2+}$ (light blue) recorded for a 5×10^{-5} M CH_2Cl_2 solution at 298 K.

Our initial evaluation of the redox properties of the complexes was carried out in dichloromethane to avoid the solvolysis problems associated with acetonitrile, and the results are summarized in Table 5. Oxidation is typically associated with the removal of an electron from a d orbital on the metal. When one tpy ligand in $[Ru(tpy)_2]^{2+}$ is substituted with bpy, water facilitates oxidation by 0.48 V, indicating that the coordinated water helps to destabilize the Ru(II) state. The substitution of binap for bpy raises the potential to >1 V, reflecting the influence of the more electronegative binap ligand, which should destabilize Ru(III). Reedijk and co-workers have observed a similar effect upon substituting 2,2′-bipyrazine for bpy in $[Ru(tpy)(bpy)Cl]^+$.[24] As the binap ligand becomes more twisted in progressing from **3a** to **3c**, this effect is less strongly felt

(20) Spek, A. L.; Gerli, A.; Reedijk, J. *Acta Crystallogr.* **1994**, *C50*, 394−397.
(21) Thummel, R. P.; Decloitre, Y. *Inorg. Chim. Acta* **1987**, *128*, 245−249.
(22) Thummel, R. P.; Lefoulon, F.; Mahadevan, R. *J. Org. Chem.* **1985**, *50*, 3824−3828.
(23) Thummel, R. P.; Hery, C.; Williamson, D.; Lefoulon, F. *J. Am. Chem. Soc.* **1988**, *110*, 7894−7896.

Table 5. Electrochemical Data for Ru(II)−Binap and Model Complexes[a]

complex	$E_{1/2}$(ox)	$E_{1/2}$(red)	
$[Ru(tpy)_2]^{2+}$	+1.30 (187)	−1.27 (110)	−1.60 (147)
$[Ru(tpy)(bpy)(H_2O)]^{2+}$	+0.82 (123)	−1.51 (130)	
$[Ru(tpy)(\mathbf{3a})(H_2O)]^{2+}$	+1.08 (80)	−0.72 (86)	−1.16 (87)
$[Ru(tpy)(\mathbf{3b})(H_2O)]^{2+}$	+1.04 (90)	−0.78 (92)	−1.21 (100)
$[Ru(tpy)(\mathbf{3c})(H_2O)]^{2+}$	+1.01 (89)	−0.83 (87)	−1.22 (93)
$[Ru(4'\text{-}NMe_2tpy)(\mathbf{3b})(H_2O)]^{2+}$	+0.87 (84)	−0.86 (85)	−1.28 (97)

[a] Half-wave potential reported in volts (V) vs SCE. The number in parentheses is the difference between the anodic and cathodic waves. Recorded at 25 °C in CH_2Cl_2 at a sweep rate of 100 mV/s, with 0.1 M TBAP as the supporting electrolyte.

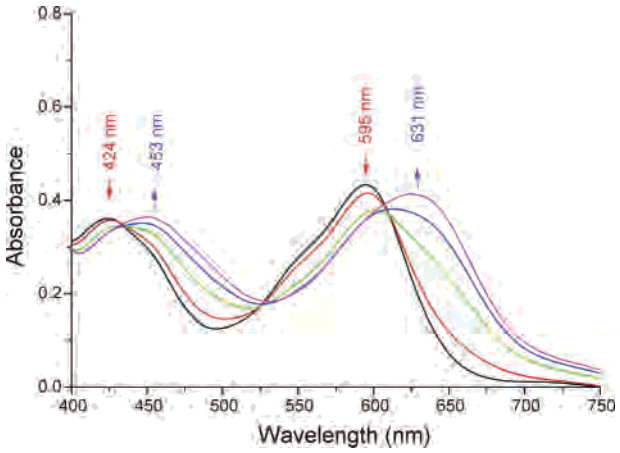

Figure 6. Titration of an acetone solution of $[Ru(tpy)(\mathbf{3b})(H_2O)]^{2+}$ (7.56×10^{-5} M) with aqueous NaOH (1.25×10^{-2} M). The equivalents of NaOH are 0 (black), 0.20 (red), 0.40 (green), 0.60 (blue), and 1.00 (purple) from Ru(II)−H_2O.

and the potential decreases by 70 mV. The incorporation of the strongly donating dimethylamino group at the tpy-4 position exerts a stabilizing effect, lowering the oxidation potential by 170 mV, and is consistent with the observation by Constable and co-workers of a 0.5 V lower oxidation potential for $[Ru(4'\text{-}NMe_2tpy)_2]^{2+}$ as compared with that of $[Ru(tpy)_2]^{2+}$.[14]

The reductions are ligand-based and correspond to the addition of an electron to the most electronegative ligand. Thus, the reduction of $[Ru(tpy)(\mathbf{3a}-\mathbf{c})H_2O]^{2+}$ complexes exhibits a steady decrease from −0.72 to −0.83 V as the ligand becomes less planar, which causes a weaker interaction with the metal center. Since these reductions are associated with the binap ligands, the incorporation of the 4′-dimethylamino group on tpy has only a relatively small effect. The second reductions occur in the range of −1.16 to −1.28 V and are likely associated with reduction of the tpy ligand, as judged by the reduction potential of −1.27 V for $[Ru(tpy)_2]^{2+}$.

There are three ways that one can perturb these Ru−aquo complexes to help better understand their properties. We can stimulate them with light, vary the external potential, or change the pH of the environment. Each of these stimuli will, in turn, influence the others, and we have undertaken a careful study of all three variables.

(24) Gerli, A.; Reedijk, J.; Lakin, M. T.; Spek, A. L. *Inorg. Chem.* **1995**, *34*, 1836−1843.

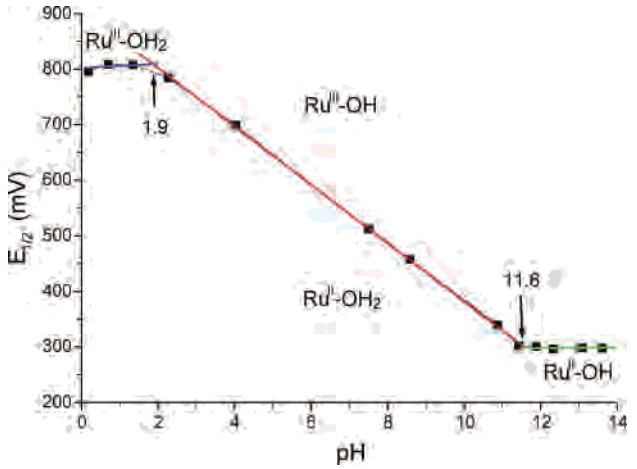

Figure 7. Pourbaix diagram for $[Ru(tpy)(\mathbf{3b})(H_2O)]^{2+}$ measured in a phosphate buffer (1.8×10^{-2} M) containing 15% acetone.

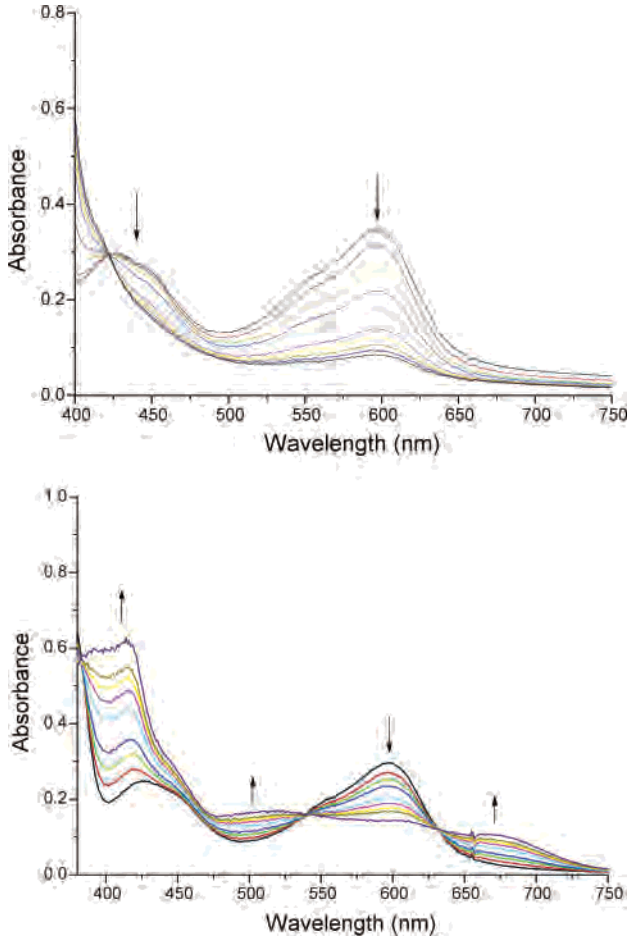

Figure 8. Oxidation of $[Ru(tpy)(\mathbf{3b})(H_2O)]^{2+}$ at 1.30 V vs SCE (top) and reduction at −0.85 V (bottom) recorded as a function of time.

When an acetone solution of $[Ru(tpy)(\mathbf{3b})(H_2O)]^{2+}$ is titrated with 1.25×10^{-2} M NaOH, the pH increases with consequent deprotonation of the bound water and generation of the Ru(II)−OH species. The MLCT absorption of this species undergoes a bathochromic shift of both the tpy and binap components, with new bands appearing at 453 and 631 nm (Figure 6). This shift to a lower energy is consistent with the idea that a hydroxide anion is better than water at stabilizing the metal dication and, thus, shifting the d−π^*

transition to a lower energy. Several isosbestic points are observed, indicating a concerted process. This process is quantitative such that the addition of 1 equiv of base leads to the complete formation of the hydroxide-bound complex.

The oxidation potential is also sensitive to changes in pH as indicated by the Pourbaix diagram shown in Figure 7. Below pH 1.9, the oxidation potential is invariant at approximately +0.81 V, indicating that under acid conditions, the water remains protonated even in the oxidized form. Above pH 11.6, the opposite is true and the water is deprotonated so that oxidation of the Ru(II)−OH species occurs at a constant potential of approximately +0.30 V. This behavior is quite similar to what Meyer and co-workers[7a] observed for the parent $[Ru(tpy)(bpy)(H_2O)]^{2+}$ complex and suggests that intramolecular deprotonation of the metal-bound water by a binap of the photoexcited complex might indeed facilitate the oxidation.

When the $[Ru(tpy)(\mathbf{3b})(H_2O)]^{2+}$ complex is either oxidized or reduced, the absorption spectrum changes dramatically, as illustrated in Figure 8. The application of a constant potential of +1.30 V causes the disappearance of both MLCT absorptions over a period of about 1 min. Reduction at −0.85 V presumably occurs on the more electronegative binap ligand, making it a much poorer charge acceptor and, hence, decreasing the absorbance at ∼600 nm. This effect redirects MLCT to the tpy ligand, and the intensity of the band at ∼430 nm increases and shifts to a higher energy.

Dilute solutions of the binap complexes were exposed to direct sunlight over a period of several days, but no significant photobleaching occurred. Knowing that oxidation from Ru(II)−OH_2 to Ru(III)−OH causes the disappearance of the MLCT absorption and, hence, the loss of color, we must conclude that photooxidation does not readily occur for these systems. Systematic variations in the structure of the complex are underway to help remedy this problem.

Acknowledgment. The authors thank the Robert A. Welch Foundation (E-621) and the Division of Chemical Sciences, Office of Basic Energy Sciences, U.S. Department of Energy (Contract DE-FG03-02ER15334), for financial support of this work. We also thank Dr. James Korp for assistance with the X-ray determinations using MRSEC/TCSUH Shared Experimental Facilities supported by the NSF under Award DMR-9632667 and the Texas Center for Superconductivity at the University of Houston. We further thank Dr. Zhongping Ou for assistance with the spectroelectrochemical experiments.

IC040051N